PNAS RESEARCH ARTICLE | DEVELOPMENTAL BIOLOGY

The CHARGE syndrome ortholog CHD-7 regulates TGF-β pathways in *Caenorhabditis elegans*

Diego M. Jofré[a,1], Dane K. Hoffman[b,1,2], Ailen S. Cervino[c], Gabriella M. Hahn[d], McKenzie Grundy[b], Sijung Yun[e], Francis R. G. Amrit[f], Donna B. Stolz[g], Luciana F. Godoy[a], Esteban Salvatore[a], Fabiana A. Rossi[h], Arjumand Ghazi[f,i,j], M. Cecilia Cirio[c], Judith L. Yanowitz[b,k,l,3], and Daniel Hochbaum[a,3]

Edited by Victor Ambros, University of Massachusetts Medical School, Worcester, MA; received June 2, 2021; accepted February 24, 2022

CHARGE syndrome is a complex developmental disorder caused by mutations in the chromodomain helicase DNA-binding protein-7 (CHD7) and characterized by retarded growth and malformations in the heart and nervous system. Despite the public health relevance of this disorder, relevant cellular pathways and targets of CHD7 that relate to disease pathology are still poorly understood. Here we report that *chd-7*, the nematode ortholog of Chd7, is required for dauer morphogenesis, lifespan determination, stress response, and body size determination. Consistent with our discoveries, we found *chd-7* to be allelic to *scd-3*, a previously identified dauer suppressor from the DAF-7/ tumor growth factor-β (TGF-β) pathway. Epistatic analysis places CHD-7 at the level of the DAF-3/DAF-5 complex, but we found that CHD-7 also directly impacts the expression of multiple components of this pathway. Transcriptomic analysis revealed that *chd-7* mutants fail to repress *daf-9* for execution of the dauer program. In addition, CHD-7 regulates the DBL-1/BMP pathway components and shares roles in male tail development and cuticle synthesis. To explore a potential conserved function for *chd-7* in vertebrates, we used *Xenopus laevis* embryos, an established model to study craniofacial development. Morpholino-mediated knockdown of Chd7 led to a reduction in *col2a1* messenger RNA (mRNA) levels, a collagen whose expression depends on TGF-β signaling. Both embryonic lethality and craniofacial defects in Chd7-depleted tadpoles were partially rescued by overexpression of *col2a1* mRNA. We suggest that Chd7 has conserved roles in regulation of the TGF-β signaling pathway and pathogenic Chd7 could lead to a defective extracellular matrix deposition.

CHARGE syndrome | *chd-7* | dauer | TGF-β | Col2a1

Significance

CHARGE syndrome is a complex developmental disorder caused by mutations in CHD7 (chromodomain helicase DNA-binding protein-7). We identified *Caenorhabditis elegans chd-7* in a screen for suppressors of dauer formation, an alternative larval stage that develops under harsh environmental conditions. We found *chd-7* regulates tumor growth factor-β (TGF-β) signaling pathways both for dauer diapause and for development of the cuticle, a specialized extracellular matrix. In frog embryos, Chd7 promotes Col2a1 expression, which is necessary and sufficient to prevent CHARGE features. These studies establish a conserved role for Chd7 from worms to vertebrates in regulating the TGF-β signaling pathway. Genetic dissection of *chd-7*'s role in *C. elegans* may help to define the molecular and cellular events that contribute to CHARGE syndrome.

When *Caenorhabditis elegans* encounter crowding, starvation, or high temperature during early development, worms can halt reproductive programs to enter an alternative larval stage, known as dauer. Dauers are long-lived, highly stress-resistant, and exhibit altered motility and metabolism (1–4). Upon return to normal growth conditions, the larvae exit dauer and develop into fertile adults. Study of dauer formation mutants has provided fundamental insights into pathways affecting longevity, neurodevelopment, metabolism, autophagy, and neurodegeneration (1, 4–7).

The DAF-2/insulin/IGF1 (IIS) signaling pathway controls the dauer entry decision by coupling external cues with neuroendocrine signaling (8). In favorable conditions, DAF-2 activity initiates a conserved kinase cascade, leading to phosphorylation and inhibition of the transcription factor DAF-16/FOXO. In harsh environments, a decrease in the activity of DAF-2 and downstream components of the pathway leads to activation of DAF-16 and causes animals to arrest as dauers (9, 10). In addition to the DAF-2 pathway, DAF-7/tumor growth factor-β (TGF-β) signaling also regulates dauer development (11). When worms sense suitable conditions for reproductive development, ASI neurosensory cells secrete the DAF-7 ligand, which binds to DAF-1/4 receptors, leading to activation and phosphorylation of the R-SMAD complex DAF-8/14, promoting reproductive programs and inhibiting the prodauer complex composed of the SMAD protein DAF-3 and repressor DAF-5. Conversely, absence of DAF-7 leads to activation of the DAF-3/DAF-5 complex to promote dauer entry (12, 13).

The DAF-7/TGF-β and DAF-2/IIS were initially described as parallel pathways to regulate dauer entry (14), but recent observations suggest a strong, positive feedback between these pathways for dauer entry and longevity (15–20). First, decreased signaling through the TGF-β pathway leads to differential expression of many DAF-16–regulated genes with functions in longevity and dauer entry, such as SOD-3 and insulin peptides. This cross-activation of target genes may be important to amplify weak signals from each sensory pathway in order to make an all-or-none decision to enter dauer (15–17). Second, the longevity of *daf-2* mutants can be blocked or

The authors declare no competing interest.

This article is a PNAS Direct Submission.

[1]D.M.J. and D.K.H. contributed equally to this work.

[2]Present address: Department of Cancer & Cell Biology, Baylor College of Medicine, Houston, TX 77030.

[3]To whom correspondence may be addressed. Email: yanowitzjl@mwri.magee.edu or hoch30@gmail.com.

This article contains supporting information online at http://www.pnas.org/lookup/suppl/doi:10.1073/pnas.2109508119/-/DCSupplemental.

Published April 8, 2022.

enhanced by *daf-5* and *daf-3*, respectively, suggesting that transcriptional components of the TGF-β pathway can modulate IIS-dependent longevity genes. Third, for dauer development, *daf-16* is epistatic to *daf-7/8/14 daf-c* mutants (17, 18). Finally, both signaling pathways converge on *daf-9* and *daf-12* to integrate outputs for diapause entry (19, 20). Indeed, *daf-9* expression levels are critical for both entering and exiting diapause (4, 19).

In chromatin immunoprecipitation (ChIP)-chip studies, we identified *chd-7* as target of DAF-12, a nuclear receptor whose loss causes defective execution of dauer morphogenesis programs (21). *chd-7* is an ortholog of *CHD7* (chromodomain-helicase-DNA binding 7), which is the primary locus associated with CHARGE syndrome, a rare and severe neurodevelopmental disorder that affects the neural tube and neural crest cell derivatives, leading to hypogonadism, heart defects, and craniofacial anomalies among other features (22). Inactivating mutations in *CHD7* are the predominant cause of CHARGE, accounting for greater than 90% of the cases (23). *CHD7* is also mutated in Kallmann syndrome, a milder neurodevelopmental disorder with features overlapping with CHARGE, including impaired olfaction and hypogonadism (24). Exome sequencing studies in patients with autism spectrum disorders identified recurrent disruptive mutations in the related gene *CHD8* (25).

The CHD proteins comprise a highly conserved family of SNF2-related ATP-dependent chromatin remodelers that are involved in chromatin remodeling and transcriptional regulation (26). Despite the public health relevance of these cognitive disorders, the mechanism of disease pathology due to mutations in CHD7/8 is poorly understood. The development of fly, fish, and mouse models of CHARGE has enabled characterization of associated dysfunction in model organisms, but our understanding of the underlying pathology of CHARGE is still incomplete (27–32). In *C. elegans*, CHD-7 has functions in habituation learning, normal locomotion, body size, and fecundity (33, 34). It contains a conserved ATPase/SNF2 domain and two chromodomains for nucleosome interaction. Being the only worm homolog of the class III CHD family, it contains a signature BRK domain (Brahma and Kismet domain) (Fig. 1*E*).

Here, we show that while CHD-7 can modulate multiple IIS-associated processes—including *daf-2(e1370)* dauer formation, longevity, and immunity—epistasis experiments place *chd-7* in the DAF-7/TGF-β pathway that impinge on IIS signaling (15). In addition, CHD-7 affects *daf-12*, *daf-14*, *daf-3*, and *daf-5* transcription levels, suggesting that it modulates the DAF-7/TGF-β pathway at multiple points. Whole-genome messenger RNA (mRNA) expression profiling of partial *chd-7;daf-2* dauers show that *chd-7* mutants fail to repress *daf-9*. We also found that CHD-7 binds and regulates *dbl-1* and *sma-2*, key components of the BMP pathway, a conserved signaling pathway that regulates cuticle collagen expression from worms to mammals (35–39).

To explore a potential conserved function for *chd-7* in vertebrates and study the relevance of our results for CHARGE etiology, we used *Xenopus laevis*. Disruption of Chd7 function in *Xenopus* embryos results in craniofacial defects that mimic CHD-dependent pathological phenotypes (40, 41). We demonstrate that Chd7 regulates expression of the collagen type-II α1 (*col2a1*), the main collagen protein of cartilage (42), whose expression depends on the TGF-β pathway (43, 44). Interestingly, craniofacial malformations and embryonic lethality due to *chd7* knockdown can be rescued by *col2a1* expression. These findings suggest a conserved function of Chd7/*chd-7* in regulation of extracellular matrix (ECM) components and raise the intriguing possibility that defects in collagen expression may contribute to the craniofacial defects seen in Chd7/8-dependent syndromes.

Results

***chd-7* Functions in Development of the Dauer Larva.** To identify novel regulators of dauer development, we previously used ChIP-chip to define DAF-12 target genes (21). Herein, we screened ∼300 targets, including *chd-7*, to determine which influenced dauer induction or morphogenesis. To identify such genes, we took advantage of the temperature-sensitive, constitutive dauer (*daf-c*) allele *daf-2(e1371)*. Inactivation of *chd-7*, which contains seven DAF-12 binding sites in its promoter region (-4600, -4564, -2837, -2776, -1944, -1273, and -361) (21), led to development of defective, SDS-sensitive "partial" dauers in *daf-2(e1371)* animals grown at the nonpermissive temperature of 25 °C (9). To confirm these results, we assayed suppression of the more severe *daf-2(e1370)* mutation and discovered that *chd-7(RNAi)* produced a similar arrested partial dauer phenotype (45). As observed in Fig. 1 *A* and *B*, the axial ratio (length/width) of the partial dauers resulting from *chd-7(RNAi)* exhibited a significant reduction of these proportions and appeared to have defects in radial constriction of the dauer cuticle. By using a *chd-7* transcriptional reporter (WBStrain00033709), we observed a substantial decrease in *chd-7* expression in the *daf-12(rh61rh411)* background (Fig. 1 *C* and *D*). Thus, we infer that the binding of DAF-12 to the *chd-7* promoter (21) up-regulates its expression.

To further validate our screen, we crossed *daf-2(e1370)* mutants with three *chd-7* deletion alleles available from the Nematode Knockout Consortia (46). *chd-7(tm6139)* contains a 594-bp deletion that generates a frame shift and premature stop codon, eliminating all known protein domains (Fig. 1*E*). As shown in Fig. 1*F*, partial dauers were obtained when double mutants are grown at 25 °C, validating our interference RNA (RNAi) screen. Comparison of two C-terminal deletion alleles uncovered a critical role for the BRK domain in dauer formation. The *chd-7(gk290)* allele contains an 859-bp deletion that spans the BRK domain and introduces a frameshift that eliminates the last 356 aa. The *chd-7(gk306)* deletion is slightly more C-terminal, truncating the protein immediately after the BRK domain (Fig. 1*E*). When crossed into *daf-2(e1370)* worms, *chd-7(gk306)* developed normal dauer larvae, whereas *chd-7(gk290)* formed partial dauers (Fig. 1*F*). Importantly, a functional transgene expressing GFP-tagged CHD-7 protein (CHD-7::GFP) rescued the partial dauer phenotypes observed in *chd-7(gk290);daf-2(e1370)* and *chd-7(tm6139);daf-2(e1370)* mutants (Fig. 1*F*).

We then aimed to understand if loss of *chd-7* also prevents normal dauer development in a *daf-2(+)* background. As shown in Fig. 1*G*, under starvation conditions that favor dauer arrest (47), N2 (wild-type) worms developed into dauers that were shorter than *daf-2(e1370)* dauers but, as expected, were resistant to SDS treatment (*SI Appendix*, Fig. S1). In contrast, *chd-7* mutants showed complex phenotypes. Most of the *chd-7(gk290)* animals arrested as L3- and L4-like larvae (Fig. 1*G* and *SI Appendix*, Fig. S1). *chd-7(tm6139)* exhibited larval arrest and mortality at the L1 stage. Of the small fraction of animals that did progress, some developed into scrawny L3-like or L4-like larvae; some progressed to adulthood. These results are consistent with the requirement for *chd-7* in the induction of dauer formation by starvation.

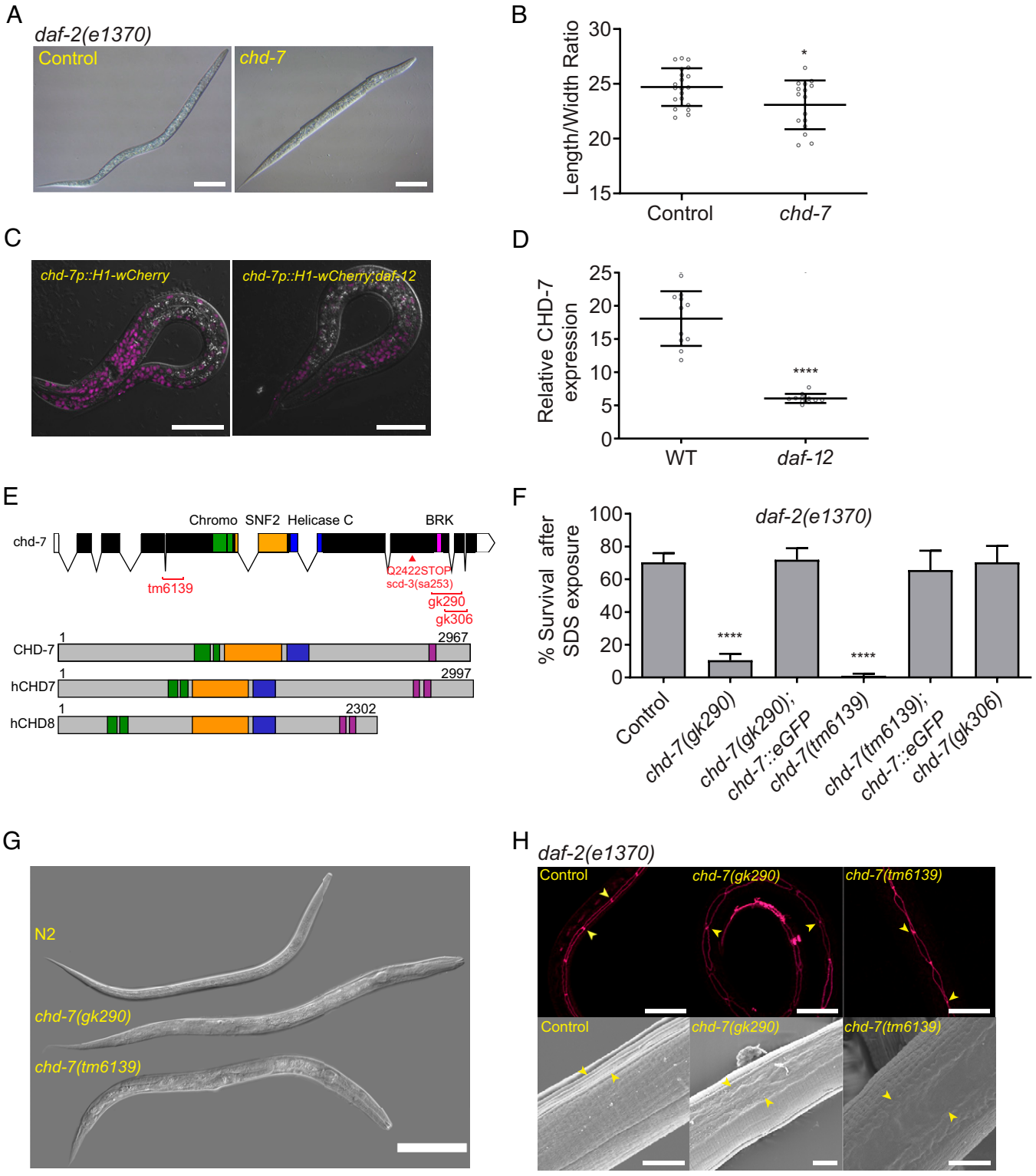

Fig. 1. The DAF-12 regulated target *chd-7* is required for proper dauer morphogenesis. (*A*) *chd-7(RNAi)* causes a partial dauer phenotype in *daf-2(e1370)*. Representative DIC photomicrographs of normal and partial dauers from *daf-2(e1370)* exposed to Control (L4440) or *chd-7* dsRNA, respectively. (Scale bars: 50 uM.) (*B*) Quantification of axial ratio of *daf-2(e1370);control(RNAi)* and *daf-2(e1370);chd-7(RNAi)* dauers. Three biological replicates were scored ($n = 16$ to 21 worms per replicate). Horizontal black lines represent mean with SD. Unpaired *t* test, $*P < 0.05$. (*C*) *daf-12* regulates *chd-7* expression. Representative images of *chd-7* transcriptional reporter, *chd-7p::H1-wCherry* or *chd-7p::H1-wCherry;daf-12(rh61rh411)* worms at L2/L3 stage. (Scale bars: 20 uM.) (*D*) Relative expression of the transcriptional reporter ($n > 10$ per strain). Unpaired *t* test, $****P < 0.0001$. (*E*) *C. elegans chd-7* gene and protein. (*Upper*) *chd-7* genomic region. UTR and exons shown as bars; introns by lines. In red, available *chd-7* deletional alleles (data obtained from *Caenorhadbitis* Genome Center and National Bioresearch Project). (*Lower*) The predicted protein isoforms of *C. elegans* CHD-7, human CHD7, and human CHD8. Signature domains in CHD proteins: two N-terminal chromodomains for interaction with a variety of chromatin components (green), a SNF-2 like domain with ATPase activity (yellow), and a helicase domain (blue). The class III subfamily is defined by a BRK domain (purple). (*F*) *chd-7*(*gk290*);*daf-2(e1370)* and *chd-7*(*tm6139*);*daf-2(e1370)* develop as SDS-sensitive dauer larvae. $n > 725$ animals per strain tested. Bars and horizontal black lines represent mean percentage with SD. χ^2 test with Bonferroni correction for multiple comparisons. $****P < 0.0001$. Asterisks represent the comparison to *daf-2(e1370)*. (*G*) *chd-7*(*gk290*) and *chd-7*(*tm6139*) prevent dauer development upon starvation of otherwise wild-type worms. Representative DIC photomicrographs of N2 dauers, arrested L3-like *chd-7*(*gk290*), and a small *chd-7*(*tm6139*) adult. (Scale bar: 100 uM.) (*H*) *chd-7;daf-2* partial dauers fail to develop the dauer alae. (*Upper*) Representative photomicrographs of *daf-2(e1370)* dauers or *chd-7;daf-2(e1370)* partial dauers expressing the *ajm-1*::GFP reporter to delineate the seam cell borders (arrowheads mark a subset of junctions). (Scale bars: 20 uM.) (*Lower*) Scanning electron microscopy images of *daf-2(e1370)* dauers or *chd-7;daf-2(e1370)* partial dauers (arrowheads mark alae details). (Scale bars: 5uM.)

The dauer larva is characterized by a slim physique because of a reduction in the volume of ectodermal tissues, including the hypodermis, seam cells, and pharyngeal cells. In addition, the hypodermis produces the dauer cuticle, which confers protection against external damage and dehydration. During wild-type dauer formation, the seam cells adopt a stereotypical linear morphology and junctional association to produce the alae, bilateral ridges in the cuticle, that facilitate body motion. Dauer larvae also switch their metabolism to accumulate lipids to survive for longer periods (10). To further characterize the nature of the defects in the *chd-7*-induced partial dauers, we analyzed the seam using the adherens junction-associated protein marker AJM-1::GFP and interrogated the morphology of the cuticle using scanning electron microscopy. As shown in Fig. 1*H*, partial dauers exhibited defects in seam cell morphology and defective dauer alae formation. During the dauer transition, animals store fat in their intestinal and hypodermal cells, which is critical to survive during hibernation (48). We used the lipid-labeling dye Oil red O to examine fat storage. Unlike other partial dauer mutants (6), *chd-7;daf-2* abnormal dauers did not exhibit fat-storage deficiencies (*SI Appendix*, Fig. S2).

During dauer, the global developmental arrest also impacts the germ cells, slowing their divisions and finally resulting in quiescence (49). We observed that the germline in *chd-7;daf-2* mutant dauers was substantially larger than in control *daf-2* dauers, arresting with a germline morphology that resembled the L3 larval stage (*SI Appendix*, Fig. S3). Therefore, we conclude that major morphological changes that occur during dauer formation of *daf-2(e1370)* fail to be executed in *chd-7* mutants, including radial constriction of the body, formation of an SDS-resistant cuticle with dauer alae, and developmental arrest of the germline.

chd-7 Is Required for Longevity and Immunoresistance Induced by IIS Inactivation and Germline Removal. In addition to dauer development, the IIS pathway also regulates longevity (1). Hence, we sought to investigate whether *chd-7* also has roles in the determination of lifespan. First, we compared survival of wild-type (N2) worms with two *chd-7* alleles and found that the dauer-defective allele *chd-7(gk290)* significantly shortened lifespan, whereas *chd-7(gk306)* had only a marginal effect on longevity (Fig. 2*A*). Surprisingly, the CHD-7::GFP rescue transgene also reduced N2 lifespan (Fig. 2*B*), suggesting that *chd-7* copy number can influence longevity. We then analyzed how *chd-7* affects longevity of IIS mutants. Remarkably, the dauer-defective allele *chd-7(gk290)*, but not *chd-7(gk306)*, shortened the lifespan extension of *daf-2* mutants to an extent comparable with the null allele of *daf-16,* the key IIS downstream target (Fig. 2*C*) (1). Furthermore, *daf-2* longevity was fully restored by CHD-7::GFP (Fig. 2*D*).

To determine if the effects on lifespan were specific to the IIS pathway, we assayed whether *chd-7* contributes to the longevity induced by germ-cell–less mutations, a longevity paradigm that operates in parallel to IIS (50). Temperature-sensitive *glp-1(e2144)* animals are sterile and long-lived at non-permissive temperatures (51). This lifespan extension was dependent on *chd-7*, as *chd-7(gk290);glp-1(e2144)* double mutants had a mean lifespan significantly shorter than *glp-1(e2144)* single mutants (Fig. 2*E*). The impact was similar to that produced by absence of the nuclear receptor *daf-12* (Fig. 2*E*), which is strictly necessary for longevity of germ-cell–less animals (51).

In addition to longevity, IIS reduction also enhances resistance against multiple stressors, including pathogen attack and starvation. We therefore tested if *chd-7* inactivation impaired *daf-2* immunoresistance. As shown in Fig. 2*F*, *chd-7* mutants repressed the increased survival of *daf-2* worms upon exposure to the human opportunistic pathogen, *Pseudomonas aeruginosa* strain PA14 (52). In contrast, *chd-7* had only a modest effect on survival of wild-type worms to pathogen. Furthermore, the *chd-7(gk290)* and *chd-7(tm6139)* alleles reduced the survival of *daf-2(e1370)* L1 larvae subjected to starvation stress (*SI Appendix*, Fig. S4) (53). Taken together, these results suggest that *chd-7* mediates the increased lifespan of at least two longevity paradigms (IIS mutants and germ-cellless animals), as well as the response to pathogens and starvation.

We then analyzed the ChIP-sequencing (ChIP-seq) datasets from CHD-7 and DAF-16 generated by ModEncode from YA/L4 larvae (Dataset S1). To our surprise, we found that both transcriptional regulators shared a significant number of genes (*SI Appendix*, Fig. S5). These data indicate that *chd-7* might modulate longevity and pathogen resistance by regulation of the IIS pathway, possibly through direct regulation of target genes or through direct regulation of *daf-16* (see below). Regulation of the IIS pathway could also be mediated by the TGF-β pathway (15), a hypothesis we examine below.

CHD-7 Functions in Multiple TGF-β Pathways. We sought to understand whether *chd-7* also modulates the TGF-β dauer pathway (14, 15). *daf-7(1372)* is dauer-constitutive at the restrictive temperature of 25 °C. As shown in Fig. 3*A*, *chd-7;daf-7(e1372)* double mutants bypassed the dauer arrest to become fertile adults at 25 °C. The downstream cofactor encoded by *daf-5* also suppresses dauer-constitutive alleles in the TGF-β pathway at 25 °C, but is diminished in its ability to suppress at slightly higher temperatures (>25.8 °C) (13). Thus, we next asked whether *chd-7* mutation also prevented the *daf-7* dauer arrest at higher temperatures. As shown in Fig. 3*A*, *chd-7* mutation could not bypass the *daf-7*–dependent arrest at higher temperatures (54). As expected for a putative transcriptional regulator, epistasis analysis placed CHD-7 downstream of the receptor DAF-1 and the R-Smad DAF-14 (Fig. 3*B*). Interestingly, at 26.5 °C, *chd-7*-defective dauers were typically surrounded by undetached cuticle (Fig. 3*C*), a phenotype previously associated with molting defects due to overexpression of *daf-9* (55). Like *chd-7;daf-2* dauers (Fig. 1*F*), *chd-7;daf-7* dauers are sensitive to SDS exposure, indicating that there are cuticle defects in this *daf-c* genetic background (Fig. 3*C*).

A second TGF-β signaling pathway regulates body size and male tail development, mainly through the ligand DBL-1 and downstream Smads (56, 57). To test if *chd-7* is required for these processes as well, we measured the length of *chd-7* young adults and found them to be significantly shorter than wild-type animals (Fig. 3*D*). We also observed that males carrying the severe loss-of-function allele *chd-7(tm6139)* failed to mate with *fog-2* mutant females due to defects in male tail development (see next paragraph) (18). This male infertility was rescued by the CHD-7::GFP transgene (Fig. 3*E*). Mating did occur with the weaker *chd-7(gk290)* allele.

More than 20 y ago, in a screen for suppressors of dauer formation within the TGF-β pathway, Inoue and Thomas (18) identified three complementation groups. We noticed that one of these, *scd-3* (suppressor of constitutive dauer-3), was located between *unc-11* and *dpy-5* on chromosome I, in the same genetic region as *chd-7*. Features of *scd-3(sa253)* worms include low brood size, egg-laying defects (Egl), short body size (Dpy), and male abnormal defects (Mab), all of which are phenotypes shared with *chd-7*, described above. In addition, improper

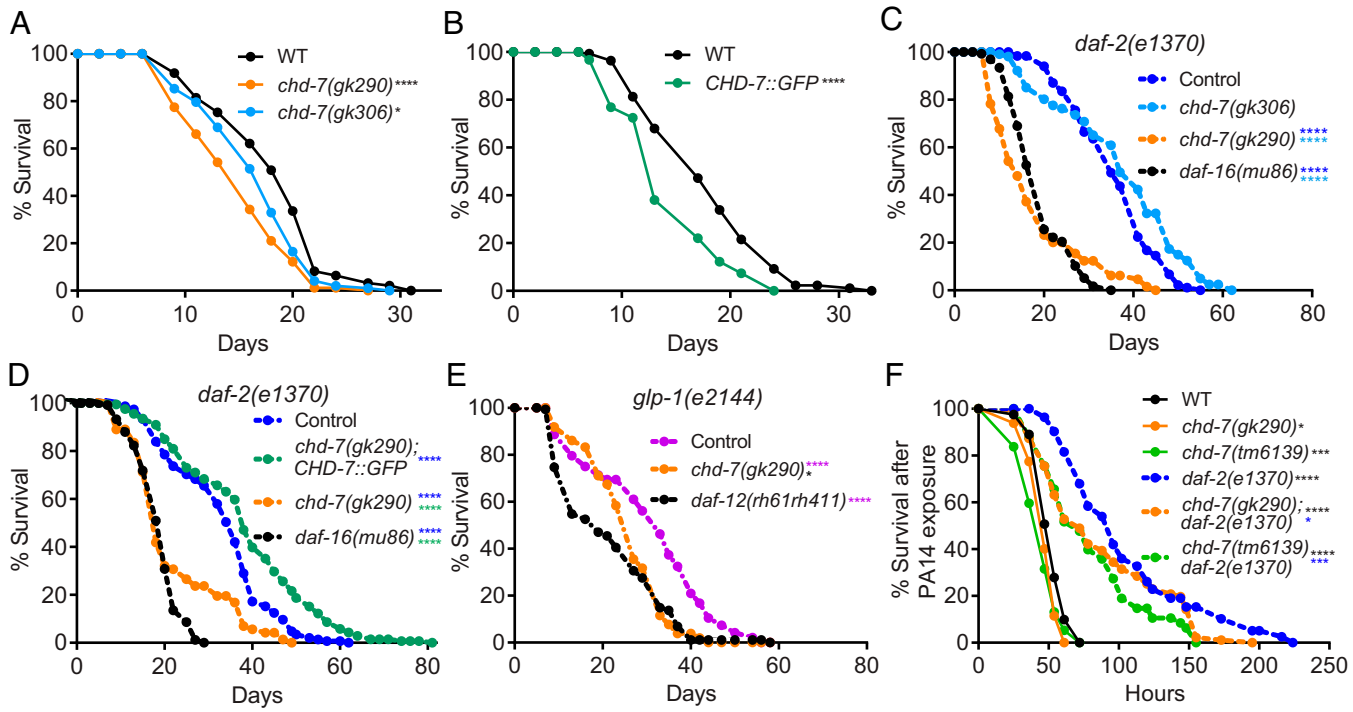

Fig. 2. *chd-7* affects longevity and response to pathogen. (*A–E*) *chd-7* promotes longevity in wild-type, *daf-2(e1370)*, and *glp-1(e2144)* mutants. Mean survival days on OP50-1; survival data analyzed using Kaplan−Meier test. For all experiments, the asterisk in color represents strain of reference for statistical analysis. Details of number of animals and additional data from replicates can be found in *SI Appendix*, Table S1. (*A*) WT (18.12), *chd-7(gk290)* (14.91), *chd-7(gk306)* (16.53). *P < 0.05 and ****P < 0.0001 compared to the wild-type, N2 strain. (*B*) WT (17.85), CHD-7::GFP (14.35). ****P < 0.0001 compared to the wild-type, N2 strain. (*C*) *daf-2(e1370)* (35.58), *chd-7(gk306);daf-2(e1370)* (37.18), *chd-7(gk290);daf-2(e1370)* (17.47), *daf-16(mu86);daf-2(e1370)* (18.85). ****P < 0.0001. (*D*) *daf-2(e1370)* (27.9), *chd-7(gk290);daf-2(e1370);CHD-7::GFP* (30.84), *chd-7(gk290);daf-2(e1370)* (19.13), *daf-16(mu86);daf-2(e1370)* (14.48). ****P < 0.0001. (*E*) *glp-1(e2144)* (30.4), *chd-7(gk290);glp-1(e2144)* (28.37), *glp-1(e2144);daf-12(rh61rh411)* (25.99). *P < 0.05 and ****P < 0.0001. (*F*) *chd-7* mediates the response against the opportunistic bacteria *P. aeruginosa*. Mean lifespan in hours (m) ± SEM. *n* is the number of animals analyzed/total number in experiment. WT (mean = 52.11 ± 0.96, *n* = 94 of 162), *chd-7(gk290)* (mean = 47.45 ± 1.05, *n* = 54 of 130), *chd-7(tm6139)* (mean = 44.47 ± 1.57, *n* = 56 of 80), *daf-2(e1370)* (mean = 105.46 ± 5.61, *n* = 65 of 115), *chd-7(gk290);daf-2(e1370)* (mean = 86.74 ± 4.21, *n* = 103 of 120), and *chd-7(tm6139);daf-2(e1370)* (mean = 79.13 ± 4.9, *n* = 50 of 60). *P < 0.05; ***P < 0.001 and ****P < 0.0001. Survival data analyzed using Kaplan−Meier test.

gonad migration is a common phenotype of *scd-3* and *chd-7(tm6139)* mutant animals (*SI Appendix*, Fig. S6). To determine if *chd-7* and *scd-3* are allelic, we sequenced *scd-3(sa253)* and found a single G/A mutation in exon 8 of the *chd-7* locus that introduces a premature STOP codon at position Q2422, eliminating the BRK domain of CHD-7 protein. This analysis confirmed that *chd-7* is *scd-3* (Fig. 1*E*).

Analysis of the male tail defect in *scd-3* mutants showed missing, deformed, and fused rays, as well as defective hook and spicules (18). These phenotypes are more severe than the typical fused rays seen in animals carrying mutations in *dbl-1*, *sma-2*, *sma-3*, and *sma-4*, which encode the ligand and downstream signaling components of the Sma/Mab pathway, respectively (56–58). Thus, while *chd-7* appears to impact many of the same developmental pathways as TGF-β mutants, the severity of its phenotypes may indicate that it has broader roles in developmental gene regulation.

***chd-7* Regulates Expression of TGF-β Pathway Components.** Our phenotypic analysis suggested that CHD-7 may influence both the DAF-7/Dauer and Sma/Mab TGF-β pathways. One possibility is that CHD-7 might directly impact expression of the pathway members. By analyzing CHD-7's CHIP-seq data from young adults generated by the ModEncode project, we noticed that CHD-7 associated with genes regions encoding TGF-β pathway components (Dataset S1). To determine whether *chd-7* is required for proper expression of these genes in vivo, we performed qRT-PCR on wild-type and *chd-7(tm6139)* L4 larvae. As shown in Fig. 3*F*, *chd-7(tm6139)* worms presented reduced expression of *dbl-1*, *daf-5*, and *daf-14* compared to N2. We also observed decreased expression of *daf-3*, although this was not identified in the ModEncode data, suggesting the effect of *chd-7* may be indirect. When we analyzed gene expression relative to *ama-1*, a different housekeeping gene, we also observed a significant down-regulation of *sma-2* and *daf-12* (*SI Appendix*, Fig. S7). This latter result raises the intriguing possibility that *chd-7* and *daf-12* may be mutually transcribed in a regulatory feedback loop, which will be an area of future investigation. The impact of *chd-7* on expression of multiple TGF-β pathway members, together with the cooccurrence of associated phenotypes, argues in favor of regulatory roles for *chd-7* in both the DAF-7/dauer and the Sma/Mab pathways.

***daf-9* and Cuticle Genes Are Misregulated in *chd-7* Mutants.** To gain further insight into the role of CHD-7 in dauer development, we performed RNA-sequencing (RNA-seq) analysis of *daf-2(e1370)* dauers and *chd-7(gk290);daf-2(e1370)* partial dauers. Differentially expressed gene (DEG) analysis revealed decreased expression of 28 genes and increased expression of 56 genes in the double mutants (Fig. 4*A* and *SI Appendix*, Table S2). Among the latter group, we found *daf-9*, encoding the cytochrome p450 that integrates inputs from TGF-β and insulin/IGF-II pathways to regulate DAF-12 activity during dauer development (59). We confirmed this increased expression of *daf-9* by qRT-PCR of *chd-7* natural dauers and *chd-7(gk290);daf-2(e1370)* partial dauers (Fig. 4*B*). We noted that the ModEncode CHD-7 ChIP-seq did not identify *daf-9* as a potential

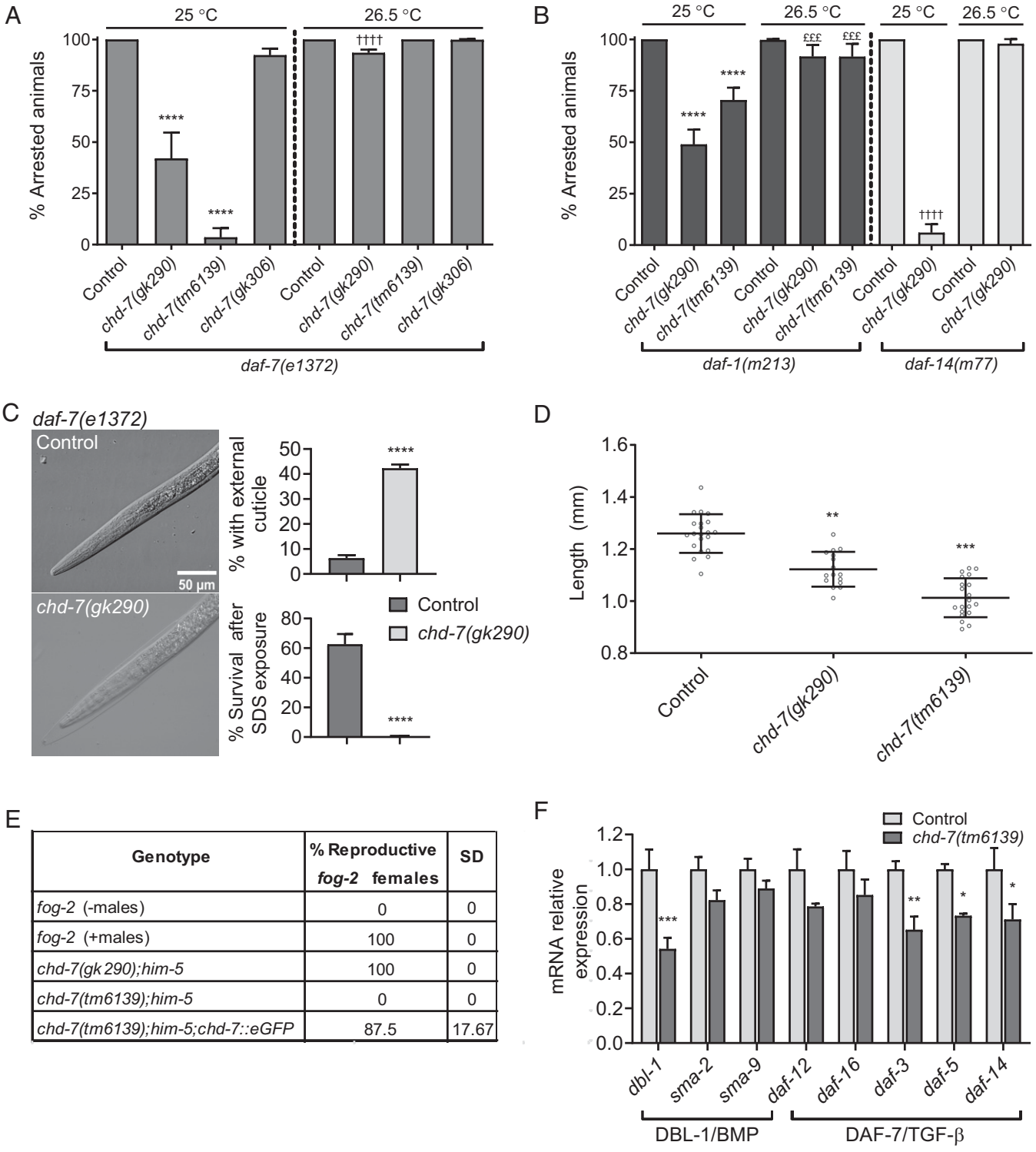

Genotype	% Reproductive *fog-2* females	SD
fog-2 (-males)	0	0
fog-2 (+males)	100	0
chd-7(gk290);him-5	100	0
chd-7(tm6139);him-5	0	0
chd-7(tm6139);him-5;chd-7::eGFP	87.5	17.67

Fig. 3. CHD-7 functions in the TGF-β signaling pathway. (*A* and *B*) Loss of *chd-7* suppresses dauer arrest of TGF-β pathway mutants at 25 °C but not 26.5 °C. Seven L4s were plated individually and grown at the specified temperature for 1 wk when arrested and nonarrested progeny were scored. Bars and horizontal black lines represent mean percentage with SD. Statistical significance was calculated using χ^2 test with Bonferroni correction for multiple comparisons. ****,$^{\dagger\dagger\dagger\dagger}P < 0.0001$ and $^{£££}P < 0.001$. (*A*) Quantification of dauer arrest in *chd-7;daf-7(e1372)* mutants. The asterisks represent comparison to *daf-7(e1372)* grown at 25 °C and the daggers represent comparison to *daf-7(e1372)* at 26.5 °C. (*B*) Dauer arrest in TGF-β pathway mutant backgrounds. The asterisks represent comparison to *daf-1(m213)* grown at 25 °C, and the daggers represent comparison to *daf-14(m77)* at 25 °C; the pound symbols represent comparison to *daf-1(m213)* at 26.5 °C. (*C*) High temperature *chd-7(gk290);daf-7(e1372)* dauers are surrounded by undetached cuticle. (*Left*) Representative DIC photomicrographs of dauers grown at 26.5 °C for 1 wk. (*Upper Right*) Quantification of the population of animals with undetached cuticle. Two biological replicates were scored ($n > 398$/replicate). (*Lower Right*) *chd-7*(*gk290*);*daf-7(e1372)* develop as SDS-sensitive dauer larvae at 26.5 °C. $n > 667$ animals per strain tested. Bars and horizontal black lines represent mean percentage with SD. Statistical analysis was calculated using two-tailed unpaired *t* test. ****$P < 0.0001$. (*D*) *chd-7* regulates body size. Body length of day 1 adults at 20 °C ($n > 16$). One-way ANOVA, **$P < 0.01$, ***$P < 0.001$ compared to wild-type, N2 strain. (*E*) *chd-7(tm6139)* males do not mate. Eight males from each strain tested were plated with four *fog-2* females on 10-cm plates. After 24 h, *fog-2* females were transferred to new plates and within 48 h the proportion of fertile females were scored. The assay was repeated twice. (*F*) Relative mRNA levels of genes from the DBL-1/BMP and DAF-7/TGF-β pathways in *chd-(tm6139)* or N2 L4s determined by qRT-PCR. Error bars indicate SE from three biological repeats. *cdc-42* was used as housekeeping gene. Statistical significance was calculated using *t* test for multiple comparisons. *$P < 0.05$, **$P < 0.01$, and ***$P < 0.001$.

target (Dataset S1). This apparent discrepancy may reflect differences in developmental timing since the ChIP-seq was performed on young adults or may suggest that *daf-9* is an indirect target of CHD-7. Nonetheless, we hypothesized that since *daf-9* expression levels are critical in the decision to either develop as fertile adults or enter diapause, the increased expression of *daf-9* in the *chd-7;daf-2* double mutants may be preventing full execution of the dauer program. Consistent with this hypothesis, we found that depletion of *daf-9* in *chd-7;daf-7* animals restored the dauer arrest phenotype at the nonpermissive temperature of 25 °C (Fig. 4*C*). However, these animals still appeared to be detergent-sensitive partial dauers (Fig. 4*D*), presumably because *daf-9* itself is required for proper dauer morphogenesis (45). Thus, we posit that the inability of *chd-7* mutants to fully repress *daf-9* may be sufficient to activate DAF-12 to promote reproductive development. Consistent with a general role for *chd-7* in regulation of *daf-9*, we also observed an undetached cuticle associated with the *chd-7(gk290);daf-7(e1372)* high-temperature dauers (Fig. 3*B*). Hypodermal *daf-9* overexpression causes a similar undetached cuticle when it bypasses starvation-induced arrest of L3 or L4 larvae (55).

Further analysis of our transcriptomic data showed that 10% of the DEGs were collagens (*col-103*, *col-50*, *dpy-2*, *col-184*, *col-141*, *col-142*, *col-42*, and *dpy-9*), which are structural components of the cuticle. All of these collagens had increased expression in the *chd-7*-mutant dauer larvae (Fig. 4*A*). Fragments per kilobase of transcript per million mapped reads data from ModEncode libraries indicates that each of these collagens shows very low expression in dauers, but are expressed during various stages of reproductive development, suggesting that the cuticle signature of partial dauers is distinct from the normal dauer cuticle . Interestingly, *col-141* and *col-142* contain SMAD-binding elements and their expression is directly regulated by DBL-1 to determine body size (35). These results could suggest the intriguing possibility that CHD-7, through regulation of the DBL-1/BMP pathway, may contribute to dauer morphogenesis by ensuring the repression of reproductive-stage cuticles.

Chd7 Regulates *col2a1* during *Xenopus* Embryogenesis. Type-II collagen is an ECM protein conserved in all multicellular animals, which forms fibrils (60) and has fundamental roles in development and tissue homeostasis (61). In vertebrates, the fibrillar type-II collagen is the major structural protein of cartilage and plays a prominent role in cranial development in multiple organisms (42, 62). Col2a1 is the major component of the cartilage matrix, having a structural function and being an important extracellular signaling molecule for regulation of chondrocyte proliferation, metabolism, and differentiation and its expression is regulated by TGF-β (43, 44, 63). The African frog *X. laevis* is a well-established model to study vertebrate facial disorders, which often arise from defects in neural crest development and migration (41). In *Xenopus* embryos, prior studies established that Chd7 regulates neural crest specification and migration and its depletion recapitulates craniofacial defects seen in CHARGE patients (40). To investigate whether a role for Chd7 in the regulation of collagen expression might be conserved in vertebrates, we used a previously validated morpholino to induce *Xenopus* Chd7 knockdown (*chd7*-MO) (40). In *Xenopus,* Col2a1 is essential for normal development of the skeleton and its expression is restricted to the cartilaginous skeleton of the tadpole and adult frog (64). In *chd7*-MO–injected embryos, qRT-PCR revealed a significant reduction of *col2a1* mRNAs as compared to the uninjected, control animals (Fig. 5*A*).

For targeted disruption of Chd7 function, we injected the dorsal-animal (D1) blastomeres of eight-cell–stage embryos fated to contribute to the dorsal anterior structures (Fig. 5*C*, schema). In situ hybridization of unilaterally injected embryos with *chd7*-MO (Fig. 5*B*, schema) showed alterations in *col2a1* expression in the branchial arches and the otic vesicle (ear vesicle) on the injected side (64). In contrast, no defects were observed in standard control morpholino (St-MO)–injected embryos (Fig. 5*B*).

The injection of *chd7*-MO into both D1 blastomeres of eight-cell–stage embryos (Fig. 5*C*, schema) induced lethality: with doses between 5 ng and 10 ng, >50% lethality was seen (Fig. 5*C*). We next sought to investigate if the mortality associated with Chd7 loss was caused by downstream effects on collagen gene expression. Therefore, we conducted rescue experiments by coexpressing *Xenopus col2a1* mRNA with the morpholino. As shown in Fig. 5*C*, coinjection of *col2a1* mRNA substantially improved (∼50%) embryo survival relative to the injection of *chd7*-MO alone.

To further interrogate the ability of ectopic *col2a1* to overcome the defects associated with *chd-7* loss, we examined the extent of the craniofacial defects in *chd7* loss-of-function. Initially, we analyzed the gross morphology of the surviving stage 45 tadpoles and observed a high incidence of craniofacial malformations (83%) in Chd7-depleted animals (*SI Appendix*, Fig. S8). These defects were significantly reduced upon *col2a1* mRNA coinjection (43%) (*SI Appendix*, Fig. S8*B*). Next, we examined eye size and eye distance, since microphthalmia and midline defects are often associated with CHARGE syndrome (65) and are recapitulated in *Xenopus* embryos (40). Both eye size and distance between eyes were reduced in *Chd7*-depleted tadpoles and were partially rescued by *col2a1* mRNA expression (Fig. 5 *D* and *E*). Therefore, expression of *col2a1* ameliorated the phenotypes associated with pathogenic Chd7, suggesting that collagen is a conserved and important target of this protein.

Discussion

We initially identified *chd-7* as a target of the nuclear receptor DAF-12 (21), a transcription factor regulating worm aging, development, and dauer formation (66). Here, we show that *chd-7* expression is up-regulated by DAF-12 and has roles in dauer development, longevity, pathogen resistance, male fertility, and body size. Our mining of ChIP-seq data and qRT-PCR analyses found decreased expression of TGF-β components in both the DAF-7/dauer and the Sma/Mab branches, indicating that *chd-7* is a regulator of the TGF-β pathways in *C. elegans* (Fig. 3*F*). While the preponderance of phenotypic and expression data supports a role for *chd-7* in the TGF-β pathways, *chd-7* might also function in TGF-β–independent mechanisms (67–69) that regulate these developmental processes.

Our genetic epistasis analyses placed CHD-7 downstream of the TGF-β–like DAF-7, the type I receptor DAF-1, and the R-SMAD DAF-14 putting CHD-7 at the level of the Co-Smad DAF-3 and the Sno/Ski repressor DAF-5, which are also Daf-d (70). Supporting a role for CHD-7 at the DAF-3/DAF-5 step in the pathway, we observed that *chd-7* completely suppressed dauer formation in a *daf-7* background at 25 °C, and like *daf-5* (13), failed to suppress dauer formation in TGF-β mutants at higher temperatures (Fig. 3 *A* and *B*). Interestingly, the *daf-3* and *daf-5* genes have opposite effects on *daf-2*–induced longevity: *daf-3* enhances *daf-2(e1370)* longevity, while *daf-5* mutations suppresse it (17). We observed that *chd-7* suppresses *daf-2* longevity (Fig. 2*C*), like *daf-5(e1386)*. Since

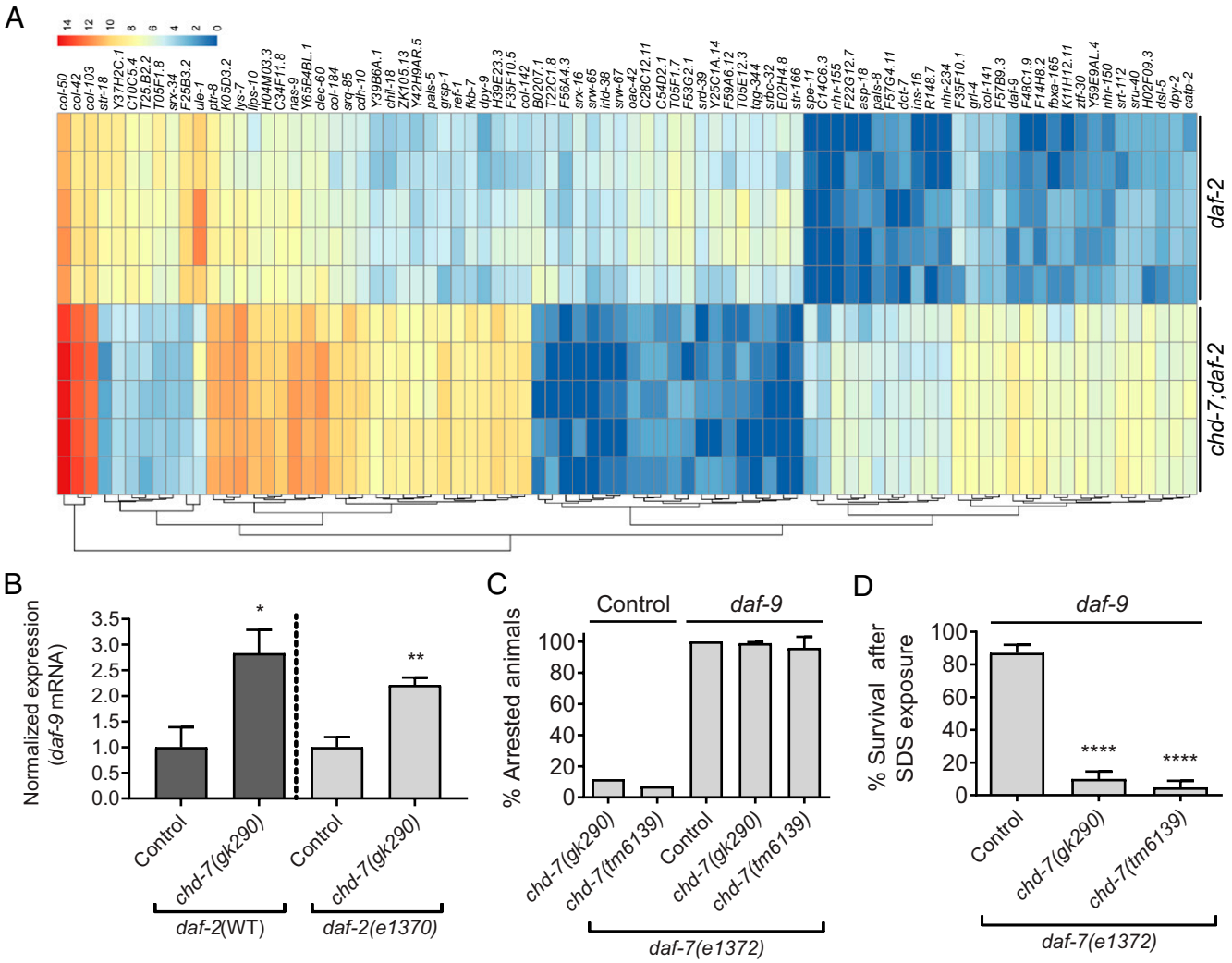

Fig. 4. RNA-seq analysis of transcriptome changes in *chd-7(gk290)* mutant dauers. (*A*) Heat map of expression values for the 84 DEGs (cutoff of 0.05 on FDR). DEGs were determined using DESeq2 (v1.20.0). The color scale represents the normalized count values in $\log_2$ scale. Hierarchical clustering of the DEGs is represented by dendrograms at bottom. (*B*) Expression levels of *daf-9* mRNA are increased in *chd-7(gk290); daf-2(e1370)* partial dauers and in L3-like arrested *chd-7(gk290)* animals upon starvation (Fig. 1*G*). Error bars indicate SE from three biological repeats. Two-tailed unpaired *t* test. $*P < 0.05$ and $**P < 0.01$. (*C*) *daf-9* knockdown in *chd-7;daf-7(e1372)* animals rescues dauer arrest at 25 °C. Two to three young L4s were plated on to freshly seeded plates with either *daf-9* or Control empty vector RNAi and allowed to lay eggs. After 72 h, the adults were removed and the proportion of progeny that arrested as dauers was calculated. Bars and horizontal black lines represent mean percentage with SD (n > 598 total animals per strain). (*D*) *daf-9* RNAi rescues arrest in *chd-7;daf-7(e1372)* animals but leads to partial dauers. Arrested animals grown at 25 °C on *daf-9* RNAi plates were treated with 1% SDS for 30 min and survival was scored. Bars and horizontal black lines represent mean percentage with SD (n > 159 total animals per strain). One-way ANOVA, $****P < 0.0001$, compared to *daf-7(e1372)*.

CHD-7 can associate with the *daf-5* locus (ModEncode ChIP-seq data), and since both *daf-3* and *daf-5* expression are reduced when *chd-7* function is compromised (Fig. 3*F*), one possibility is that CHD-7 simply functions to ensure proper expression of these critical TGF-β dauer regulators. However, CHD-7 may also directly interact with the DAF-3/DAF-5 complex to regulate downstream target genes. In mice, CHD7 was shown to physically interact with SMAD1 and form a transcriptional complex with SMAD4, the mammalian ortholog of DAF-3 (71). We therefore speculate that DAF-3, DAF-5, and CHD-7 may be in a ternary complex that regulates *daf-9* expression for dauer entry. Interactome mapping of the TGF-β pathway previously identified SWSN-1, a SWI/SNF subunit component of the BAF complex, as a physical interactor of DAF-3 (72). CHD7 interacts with human and *Xenopus* PBAF (polybromo- and BRG1-associated factor-containing complex) to control neural crest genes expression (40). In worms, both *swsn-1* and *chd-7* fail to develop normal dauers in *daf-2* and *daf-7* mutants (73) (*SI Appendix*, Fig. S9). Thus, we envision that CHD-7 may work together with the BAF complex and DAF-3/DAF-5 to control gene expression of target genes critical for dauer formation.

DAF-9 activity is a critical determinant of the decision to enter diapause: reduced activity of TGF-β and IIS pathways leads to *daf-9* repression and dauer entry. Conversely, *daf-9* expression in the hypodermis is sufficient to inhibit diapause, driving reproductive programs in *daf-7* mutants (16, 19). Ectopic *daf-9* expression also drives reproductive programs in the weak *daf-2(e1368)* allele, but only partially suppresses *daf-2(e1370)* diapause, leading to arrest as L3 or early L4 larvae (19). Based on these observations, we speculate that *daf-9* misexpression explains a subset of the *chd-7* phenotypes observed herein, including the partial dauer phenotype, gonad migration defects, and vulval protrusions, all of which overlap with published *daf-9* phenotypes (19, 20, 74). Interestingly, *daf-9* is both upstream and downstream of *daf-12* for dauer formation

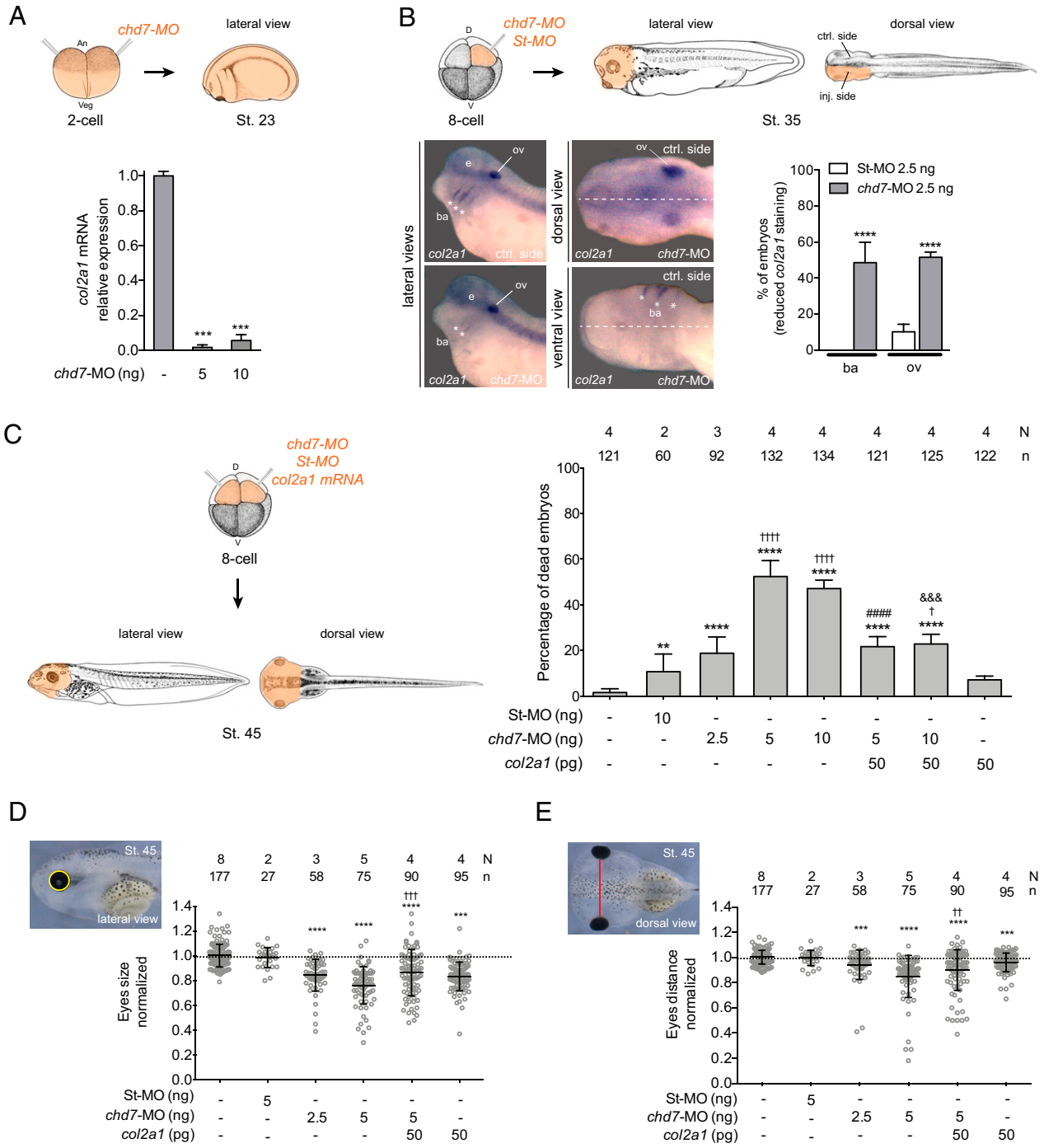

Fig. 5. Expression of *col2a1* rescues Chd-7 knockdown in *Xenopus* embryos. (*A*) Expression levels of *col2a1* mRNA are reduced in *chd7*-MO–injected embryos. Both blastomeres of two-cell–staged embryos were injected with 5 or 10 ng of *chd7*-MO and processed for RNA extraction at stage 23 (St. 23) (schematic above). Error bars indicate SE from two repeats of the PCR with different biological samples. One-tailed paired *t* test, ***$P < 0.001$. (*B*) *col2a1* expression domain is altered in the branchial arches (ba) and otic vesicle (ov) of Chd7-depleted embryos. In situ hybridization of stage 35 embryos for *col2a1*. One D1 blastomere of eight-cell–staged embryos was injected with 2.5 ng of St-MO or *chd7*-MO (schematic above) ($N = 2$; 42 and $n = 3$; 71, respectively) (N = number of experiments; n = number of embryos). Lateral, dorsal, and ventral views, anterior to the left. e: eye. Lateral views: *Upper* and *Lower* are control (ctrl) and *chd7*-MO injected sides of the same representative injected embryo, respectively. Dorsal and ventral views: white dashed lines show the middle line of the embryo. Comparisons were done between the injected side and the contralateral control side of the same embryo (schematic above). The graph is a quantification of the results. Reduced *col2a1* staining was observed in 18% of St-MO and 77% of *chd7*-MO–injected embryos that survived through stage 35. Data on graph is presented as means with SE. Fisher's exact test (****$P < 0.0001$). Asterisks represent comparison to St-MO group. (*C*) Lethality in Chd7-depleted embryos is rescued by overexpression of *col2a1*. Graph showing the percentage of dead embryos by stage 45. Both D1 blastomeres of eight-cell–staged embryos were injected as indicated in the graph and scored for survival at stage 45 (schematically depicted above). Data on graph is presented as means with SE. Fisher's exact test ($^{\dagger}P < 0.05$, **$P < 0.01$, $^{\&\&\&}P < 0.001$, ****,††††,$^{\#\#\#\#}P < 0.0001$). Asterisks represent comparison to uninjected group; daggers represent comparison to St-MO group; pound and ampersands represent comparison to *chd7*-MO 5 ng and 10 ng, respectively. (*D* and *E*) Craniofacial morphometric analysis of *Xenopus* tadpoles at stage 45. Embryos were injected as indicated in *C*. Each dot represents a single embryo. Means and SD are indicated. One-way ANOVA and Tukey's multiple comparisons test. (*D*) Quantification of the eye size (*Upper Left*). ***,$^{\dagger\dagger\dagger}P < 0.001$, ****$P < 0.0001$. (*E*) Quantification of the eye distances (*Upper Left*). $^{\dagger\dagger}P < 0.01$, ***$P < 0.001$, ****$P < 0.0001$. Lateral views, anterior to the left. Asterisks represent comparison to uninjected group and daggers represent comparison to *chd7*-MO 5-ng injected group. N = number of experiments, n = number of embryos. The source of *Xenopus* stage illustrations in *A*–*C* is Xenbase (https://www.xenbase.org/entry/, RRID:SCR_003280). *Xenopus* illustrations ©: Natalya Zahn (90) and by Nieuwkoop and Faber (86). The 12.5x and 20X digital magnification zoom of Leica L2 stereoscope were used for images in *B*. The 12.5x digital magnification was used for images in *D* and *E*.

(19, 20). Our identification of *chd-7* as both a downstream target of DAF-12 (21) and as an upstream component of the regulatory pathway that promotes DAF-12 expression suggests that these two genes may function in a regulatory feedback loop. Further dissection of the tissue- and temporal-specific requirements for these proteins is likely to further illuminate the interplay between these proteins. Notably, DAF-12 and CHD-7 both bind to sites in *daf-5*, *daf-14*, *daf-16*, *daf-12*, and *daf-19* (21) (Dataset S1), suggesting that they could coregulate expression of target genes as a transcriptional complex. We speculate that the mutual regulation between *chd-7* and *daf-12* might be important to maintain the stoichiometry of this complex. In addition, the identification of shared binding sites in *daf-16* provides a possible mechanism for the impact of *chd-7* on the IIS pathway.

Both *chd-7* mutation and *chd-7* overexpression shortened the lifespan of otherwise wild-type worms, suggesting that CHD-7 protein levels must be tightly regulated to ensure proper development. Of note, Chd7 is the most commonly amplified gene in tumors among the CHD superfamily members, and its overexpression is associated with aggressive subtypes of breast cancer and poor prognosis (75). In glioblastoma cells, Chd7 overexpression leads to a 3×-fold down-regulation of BMPR1B, vertebrate's ortholog of SMA-6 and DAF-1 (76). Thus, it's possible that the TGF-β signaling pathway, which regulates longevity, is negatively impacted in worms overexpressing CHD-7. We note that autoregulatory roles for CHD-7 during adult life, as proposed for dauer, might also explain how overexpression could be pathogenic.

It was well-established that in multiple systems, TGF-β stimulates ECM deposition mainly by promoting expression of fibronectin, collagens, and other ECM components (37, 77, 78). In addition, TGF-β promotes the synthesis of inhibitors to enzymes that degrade the ECM, including the plasminogen activator inhibitor 1 (PAI-1) and the tissue inhibitor of matrix metalloproteinases (79, 80). Mutations in the TGF-β ligand *dbl-1* and its downstream receptor and signaling components result in small body size due to transcriptional misregulation of cuticle collagen genes (35, 56, 57). Consistent with a role for CHD-7 in regulation of *dbl-1* and *sma-2* expression, *chd-7(gk290)* and *chd-7(tm6139)* are significantly shorter than wild-type worms (Fig. 3 *D* and *F*). In *Xenopus*, we show a role for Chd7 in regulating *col2a1* expression, a type II collagen and the major component of cartilage (62). Interestingly, regulation of *col2a1* by Chd7 is also observed in zebrafish (81). While additional studies are required, we speculate that Chd7 could regulate *col2a1* in a complex with the transcription factor Sox10 (82, 83) or through the TGF-β signaling pathway (37, 39). Supporting the latter mechanism, it was demonstrated in chondrocytes that TGF-β regulates *col2a1* expression (43, 44). Therefore, our results suggest that these evolutionary conserved helicases have roles in ECM deposition, supporting a model in which collagen misexpression by pathogenic Chd7 leads to craniofacial defects and embryonic lethality.

Comparison of the *chd-7* alleles *gk290* and *gk306* showed a critical role for the BRK domain in dauer development and longevity (Figs. 1 *F–H* and 2 *A*, *C*, and *E*). In CHARGE patients, deletions or mutations within the BRK domains of CHD7 are sufficient to elicit all the features characteristic of the disease, underscoring the importance of this domain (84). The phenotypic differences between the worm alleles highlight the potential of the worm to delimit functional domains of CHD-7 that contribute to disease pathology. In mice, homozygous mutations in *Chd7* lead to embryonic lethality at embryonic day 10.5, in part because *Chd7* is necessary for early brain development (40). In worms, the presumptive null alleles *chd-7(tm6139)* and *scd-3(sa253)* were viable but showed reproductive defects, such as improper gonad proliferation and migration, reduced fecundity, male tail defects, and hermaphrodite vulval defects (18), indicating that *C. elegans* are more able to tolerate loss of CHD-7 than mice or humans. Thus, our studies establish *C. elegans* as an animal model to study the mechanisms underlying the developmental defects observed in pathogenic Chd7.

Materials and Methods

***C. elegans* Strains.** Strains utilized in this study are listed in *SI Appendix*, Table S3. Standard genetic crosses were used to make double or triple mutants. The presence of mutant alleles was confirmed 1) by the *daf-c* phenotypes in animals heterozygous for additional mutations and 2) by PCR and sequencing for all additional mutations. Details for RNAi screen for dauer suppresors can be found in *SI Appendix*.

RNAi Screen for Dauer Suppressors. All RNAi clones were picked from the Ahringer bacterial feeding library. These *E. coli* clones were seeded on NGM plates supplemented with 1 mM of IPTG (Isopropyl β-D-1-thiogalactopyranoside) and 0.1 μg/mL ampicillin, and used for inducing RNAi by the feeding method.

GL228 [rrf-3(pk1426)] II;daf-2(e1371) III] eggs were placed in 24-well RNAi plates seeded with bacteria expressing the double-stranded RNA (dsRNA) of interest. Worms were maintained for 5 d at 15 °C until adulthood, then were transferred to an identical 24-well plate to lay eggs for 5 h. Adults were removed and the eggs were incubated at 25 °C for 4 d to allow formation of dauers. daf-16(RNAi) and the empty vector were used as controls. Proper dauer formation was assessed by observation in a dissecting microscope and by 1% SDS resistance. RNAi clones that caused abnormal dauer phenotypes were validated in daf-2(e1370) worms. Identity of the dsRNA was confirmed by sequencing (Macrogen).

Dauer Formation in Liquid Media. We obtained dauers in liquid media following a protocol recently described (47). Details can be found in *SI Appendix*.

***daf-9* Suppression Assays.** L4-stage animals were placed on 3-cm *daf-9(RNAi)* plates (see *SI Appendix* for preparation details). Two worms per plate were used for *daf-7(e1372)*, while three worms were used for *daf-7;chd-7(gk290)* and *daf-7;chd-7(tm6139)*. After 72 h, the adults were removed, and plates were replaced at 25 °C for 2 to 3 d. The total number of dauers, L4s, and adults were then assessed.

SDS Survival Assay. Young adults were transferred to seeded plates and permitted to lay eggs for 5 d at 25 °C. The arrested progeny were then washed off plates with M9 (22 mM KH_2PO_4, 42 mM Na_2HPO_4, 85.5 mM NaCl, 1 mM $MgSO_4$) into 15-mL glass conical tubes. Collected animals were washed two to three times with M9 and the excess liquid was aspirated off. Animals were then treated with 2 mL of 1% SDS for 30 min on a nutator at 25 °C. Following incubation, the samples were washed three times with M9 and any excess liquid was aspirated. Animals were aliquoted to five seeded plates with 50 to 70 worms per plate and allowed to recover at 16 °C. The recovered animals were then quantified, and the percentage recovered was calculated. This was repeated three times for each strain tested.

Microscopy and Fluorescence Imaging. Different imaging modalities were used for fluorescent, DIC, and EM. Details for preparation and visualization can be found in *SI Appendix*.

Lifespan Assays. All lifespan experiments were conducted by transferring 1-d-old adults from 15 °C to 20 °C for the remainder of the lifespan assay. NGM plates were seeded with E. coli OP50-1. ~150 L4 hermaphrodites were transferred to five plates per experiment. Every 48 h, animals were scored as alive, dead, or censored (animals that exploded, died from bagging or dried out at the edges of the plates). Animals were considered dead when they did not respond to a soft touch to the head with a pick. To prevent the progeny from interfering with the assay, adults were transferred to fresh plates every 48 h until egg

production ceased. For glp-1(e2144) assays, eggs were kept at 20 °C for 4 h and then transferred at 25.5 °C for 72 h to induce sterility and switched to 20 °C for the remainder of the experiment. Lifespan data were analyzed using the Kaplan–Meier method. Statistics were calculated using the Mantel–Cox nonparametric log-rank method using OASIS2 (85).

Library Preparation and RNA-Seq. *daf-2(e1370)* and *chd-7(gk290);daf-2(e1370)* synchronized eggs were kept at 25 °C for 10 d and resulting dauers were collected and frozen. Total RNA was extracted with TRIzol (Invitrogen) following the kit's protocol. The cDNA library was prepared with NEBNext Ultra II RNA library prep kit for Illumina (New England Biolabs), and the sequencing carried out using Illumina's HiSeq-2500 sequencer with single-end mode and read length of 50 bp. Five replicates for *daf-2(e1370)* vs. *chd-7(gk290);daf-2(e1370)* were sequenced. For data assessment, a quality control with FastQC software (v0.11.5) was used. First, the raw reads that aligned against the *E. coli* genome (K12 genome) were removed. The remaining sequences were aligned against the reference genome of *C. elegans* WS260 using STAR (v2.5.4a). The number of mapped reads to genes was counted using Htseq (v0.9.1). Finally, the DEGs were determined using DESeq2 (v1.20.0) with a cutoff of 0.05 on false discovery rate (FDR). R v3.5.0 (2018-04-23) and Bioconductor v3.7 with BiocInstaller v1.30.0 were used. Principal component analysis was performed using plotPCA function in DESEQ2 package. For visualization in two dimensions, we used the top two principal component axes, PC1 and PC2 (*SI Appendix*, Fig. S10). Heatmaps were generated using pheatmap package (v1.0.12) with hierarchical clustering on the rows with the default options.

***X. laevis* Embryo Manipulation and Microinjections.** *Xenopus* embryos were obtained by natural mating. Adult frogs' reproductive behavior was induced by injection of human chorionic gonadotropin hormone. Embryos were collected, de-jellied in 3% cysteine (pH 8.0), maintained in 0.1× Marc's Modified Ringer's (MMR) solution, and staged according to Nieuwkoop and Faber (86). The embryos were placed in 3% ficoll prepared in 1× MMR for microinjection. Chd7 morpholino (*chd7*-MO: 5′-AACTCATCATGCCAGGGTCTGCCAT-3′) specificity has been previously characterized (40). *Chd7*-MO and St-MO were provided by Gene Tools. The cDNA of *X. laevis col2a1* was amplified by PCR from pCMV-Sport 6-*col2a1* (Dharmacon) with primers M13F and M13R. The PCR fragment was digested with EcoRV and NotI and cloned into pCS2^{+} previously digested with StuI and NotI. Capped mRNAs for *col2a1* were transcribed in vitro with SP6 using the mMessage mMachine kit (Ambion) following linearization with NotI. Morpholinos and *col2a1* mRNA were injected into both D1 blastomeres of eight-cell staged embryos (81, 87) for lethality and morphometrics analysis. *Chd7*-MO was injected into one D1 blastomeres of eight-cell staged embryos for analysis of *col2a1* expression. For the evaluation of *col2a1* staining in the branchial arches and the otic vesicle, the injected side was compared against the contralateral control side of the same embryo. Whole-mount in situ hybridization was carried out as previously described (88) and specific details can be found in *SI Appendix*.

Ethics Statement. *X. laevis* experiments were carried out in strict accordance with *Guide for the Care and Use of Laboratory Animals* of the NIH (89) and the ARRIVE (Animal Research: Reporting of In Vivo Experiments) guidelines. The animal care protocol was approved by the Comisión Institucional para el Cuidado y Uso de Animales de Laboratorio of the School of Applied and Natural Sciences, University of Buenos Aires, Argentina (Protocol #64).

Data Availability. All study data are included in the main text and supporting information. RNA-seq data has been uploaded to National Center for Biotechnology Information Gene Expression Omnibus, ID GSE199192.

ACKNOWLEDGMENTS. The authors thank Bruno Moretti, Hernan Grecco, Mario Rossi, and Julie Kocherzat for experimental support. D.M.J., A.S.C., and L.F.G. were supported by the Consejo Nacional de Investigaciones Científicas y Técnicas (CONICET) Doctoral Fellowship Program. The D.H. laboratory was supported by the Agencia Nacional de Promoción Científica y Tecnológica of Argentina (PICT-2016-0269) and CONICET (PIP 1122015 0100731 CO). The M.C.C. laboratory was supported by the Agencia Nacional de Promoción Científica y Tecnológica of Argentina (PICT-2013-0381). Funding for this work was also provided by grants from the CHARGE Syndrome Foundation (to J.L.Y. and D.H.), The Company of Biologists (D.M.J.), National Institute of General Medical Sciences R01GM104007 (to J.L.Y.), and National Institute on Aging R01AG051659 (to A.G.). This work was supported in part by the Intramural Research Program of the NIH and the National Institute of Diabetes and Digestive and Kidney Diseases (S.Y.). Some strains used in this study were obtained from the *Caenorhabditis* Genome Center housed at the University of Minnesota and supported by a grant from the NIH Office of Research Infrastructure Programs (P40 OD010440).

Author affiliations: [a]Departamento de Biodiversidad y Biología Experimental, Facultad de Ciencias Exactas y Naturales, Universidad de Buenos Aires, C1053 Buenos Aires, Argentina; [b]Magee-Womens Research Institute, Pittsburgh, PA 15213; [c]Instituto de Fisiología, Biología Molecular y Neurociencias, Consejo Nacional de Investigaciones Científicas y Técnicas de Argentina, Facultad de Ciencias Exactas y Naturales, Universidad de Buenos Aires, C1053 Buenos Aires, Argentina; [d]Interdisciplinary Biomedical Graduate Program, University of Pittsburgh School of Medicine, Pittsburgh, PA 15213; [e]Laboratory of Molecular Biology, National Institute of Diabetes and Digestive and Kidney Diseases, National Institutes of Health, Bethesda, MD 20814; [f]Department of Pediatrics, University of Pittsburgh School of Medicine, Pittsburgh, PA 15213; [g]Center for Biologic Imaging, University of Pittsburgh Medical School, Pittsburgh, PA 15213; [h]Instituto de Investigaciones en Medicina Traslacional, Consejo Nacional de Investigaciones Científicas y Técnicas de Argentina, Universidad Austral, B1630 Pilar, Argentina; [i]Department of Developmental Biology, University of Pittsburgh School of Medicine, Pittsburgh, PA 15213; [j]Department of Cell Biology & Physiology, University of Pittsburgh School of Medicine, Pittsburgh, PA 15213; [k]Department of Obstetrics, Gynecology & Reproductive Sciences, University of Pittsburgh, Pittsburgh, PA 15213; and [l]Hillman Cancer Center, University of Pittsburgh, Pittsburgh, PA 15213

Author contributions: D.M.J., D.K.H., A.S.C., S.Y., A.G., M.C.C., J.L.Y., and D.H. designed research; D.K.H., A.S.C., G.M.H., M.G., S.Y., F.R.G.A., D.B.S., L.F.G., E.S., F.A.R., J.L.Y., and D.H. performed research; J.L.Y. and D.H. contributed new reagents/analytic tools; D.M.J., D.K.H., A.S.C., S.Y., M.C.C., J.L.Y., and D.H. analyzed data; and J.L.Y. and D.H. wrote the paper.

1. C. Kenyon, J. Chang, E. Gensch, A. Rudner, R. Tabtiang, A *C. elegans* mutant that lives twice as long as wild type. *Nature* **366**, 461–464 (1993).
2. P. L. Larsen, Aging and resistance to oxidative damage in *Caenorhabditis elegans*. *Proc. Natl. Acad. Sci. U.S.A.* **90**, 8905–8909 (1993).
3. M. M. Gaglia, C. Kenyon, Stimulation of movement in a quiescent, hibernation-like form of *Caenorhabditis elegans* by dopamine signaling. *J. Neurosci.* **29**, 7302–7314 (2009).
4. J. Wang, S. K. Kim, Global analysis of dauer gene expression in *Caenorhabditis elegans*. *Development* **130**, 1621–1634 (2003).
5. E. Cohen, J. Bieschke, R. M. Perciavalle, J. W. Kelly, A. Dillin, Opposing activities protect against age-onset proteotoxicity. *Science* **313**, 1604–1610 (2006).
6. A. Meléndez *et al.*, Autophagy genes are essential for dauer development and life-span extension in *C. elegans*. *Science* **301**, 1387–1391 (2003).
7. R. Christensen, L. de la Torre-Ubieta, A. Bonni, D. A. Colón-Ramos, A conserved PTEN/FOXO pathway regulates neuronal morphology during *C. elegans* development. *Development* **138**, 5257–5267 (2011).
8. C. A. Wolkow, K. D. Kimura, M.-S. Lee, G. Ruvkun, Regulation of *C. elegans* life-span by insulinlike signaling in the nervous system. *Science* **290**, 147–150 (2000).
9. R. C. Cassada, R. L. Russell, The dauerlarva, a post-embryonic developmental variant of the nematode *Caenorhabditis elegans*. *Dev. Biol.* **46**, 326–342 (1975).
10. P. J. Hu, Dauer, "The *C. elegans* research community" in *WormBook (August 8, 2007)*. https://doi.org/10.1895/wormbook.1.144.1. Accessed 29 March 2022.
11. P. Ren *et al.*, Control of *C. elegans* larval development by neuronal expression of a TGF-beta homolog. *Science* **274**, 1389–1391 (1996).
12. D. Park, A. Estevez, D. L. Riddle, Antagonistic Smad transcription factors control the dauer/non-dauer switch in *C. elegans*. *Development* **137**, 477–485 (2010).
13. L. S. da Graca *et al.*, DAF-5 is a Ski oncoprotein homolog that functions in a neuronal TGF beta pathway to regulate *C. elegans* dauer development. *Development* **131**, 435–446 (2004).
14. J. H. Thomas, D. A. Birnby, J. J. Vowels, Evidence for parallel processing of sensory information controlling dauer formation in *Caenorhabditis elegans*. *Genetics* **134**, 1105–1117 (1993).
15. W. M. Shaw, S. Luo, J. Landis, J. Ashraf, C. T. Murphy, The *C. elegans* TGF-β Dauer pathway regulates longevity via insulin signaling. *Curr. Biol.* **17**, 1635–1645 (2007).
16. T. Liu, K. K. Zimmerman, G. I. Patterson, Regulation of signaling genes by TGFbeta during entry into dauer diapause in *C. elegans*. *BMC Dev. Biol.* **4**, 11 (2004).
17. S. D. Narasimhan *et al.*, PDP-1 links the TGF-β and IIS pathways to regulate longevity, development, and metabolism. *PLoS Genet.* **7**, e1001377 (2011).
18. T. Inoue, J. H. Thomas, Suppressors of transforming growth factor-beta pathway mutants in the *Caenorhabditis elegans* dauer formation pathway. *Genetics* **156**, 1035–1046 (2000).
19. B. Gerisch, A. Antebi, Hormonal signals produced by DAF-9/cytochrome P450 regulate *C. elegans* dauer diapause in response to environmental cues. *Development* **131**, 1765–1776 (2004).
20. H. Y. Mak, G. Ruvkun, Intercellular signaling of reproductive development by the *C. elegans* DAF-9 cytochrome P450. *Development* **131**, 1777–1786 (2004).
21. D. Hochbaum *et al.*, DAF-12 regulates a connected network of genes to ensure robust developmental decisions. *PLoS Genet.* **7**, e1002179 (2011).
22. L. E. L. M. Vissers *et al.*, Mutations in a new member of the chromodomain gene family cause CHARGE syndrome. *Nat. Genet.* **36**, 955–957 (2004).
23. R. Balasubramanian *et al.*, Functionally compromised CHD7 alleles in patients with isolated GnRH deficiency. *Proc. Natl. Acad. Sci. U.S.A.* **111**, 17953–17958 (2014).
24. H.-G. Kim *et al.*, Mutations in CHD7, encoding a chromatin-remodeling protein, cause idiopathic hypogonadotropic hypogonadism and Kallmann syndrome. *Am. J. Hum. Genet.* **83**, 511–519 (2008).

25. R. Bernier *et al.*, Disruptive CHD8 mutations define a subtype of autism early in development. *Cell* **158**, 263–276 (2014).
26. C. G. A. Marfella, A. N. Imbalzano, The Chd family of chromatin remodelers. *Mutat. Res.* **618**, 30–40 (2007).
27. S. A. Patten *et al.*, Role of Chd7 in zebrafish: A model for CHARGE syndrome. *PLoS One* **7**, e31650 (2012).
28. E. A. Bosman *et al.*, Multiple mutations in mouse Chd7 provide models for CHARGE syndrome. *Hum. Mol. Genet.* **14**, 3463–3476 (2005).
29. C. Tian *et al.*, Otitis media in a new mouse model for CHARGE syndrome with a deletion in the Chd7 gene. *PLoS One* **7**, e34944 (2012).
30. G. Daubresse *et al.*, The Drosophila kismet gene is related to chromatin-remodeling factors and is required for both segmentation and segment identity. *Development* **126**, 1175–1187 (1999).
31. D. J. Melicharek, L. C. Ramirez, S. Singh, R. Thompson, D. R. Marenda, Kismet/CHD7 regulates axon morphology, memory and locomotion in a Drosophila model of CHARGE syndrome. *Hum. Mol. Genet.* **19**, 4253–4264 (2010).
32. Z. Asad *et al.*, Rescue of neural crest-derived phenotypes in a zebrafish CHARGE model by Sox10 downregulation. *Hum. Mol. Genet.* **25**, 3539–3554 (2016).
33. T. A. McDiarmid *et al.*, Systematic phenomics analysis of autism-associated genes reveals parallel networks underlying reversible impairments in habituation. *Proc. Natl. Acad. Sci. U.S.A.* **117**, 656–667 (2020).
34. W.-R. Wong *et al.*, Autism-associated missense genetic variants impact locomotion and neurodevelopment in *Caenorhabditis elegans*. *Hum. Mol. Genet.* **28**, 2271–2281 (2019).
35. U. Madaan *et al.*, BMP signaling determines body size via transcriptional regulation of collagen genes in *Caenorhabditis elegans*. *Genetics* **210**, 1355–1367 (2018).
36. U. Madaan *et al.*, Feedback regulation of BMP signaling by *Caenorhabditis elegans* cuticle collagens. *Mol. Biol. Cell* **31**, 825–832 (2020).
37. R. A. Ignotz, J. Massagué, Transforming growth factor-beta stimulates the expression of fibronectin and collagen and their incorporation into the extracellular matrix. *J. Biol. Chem.* **261**, 4337–4345 (1986).
38. C. H. Streuli, C. Schmidhauser, M. Kobrin, M. J. Bissell, R. Derynck, Extracellular matrix regulates expression of the TGF-beta 1 gene. *J. Cell Biol.* **120**, 253–260 (1993).
39. A. B. Roberts, B. K. McCune, M. B. Sporn, TGF-β: Regulation of extracellular matrix. *Kidney Int.* **41**, 557–559 (1992).
40. R. Bajpai *et al.*, CHD7 cooperates with PBAF to control multipotent neural crest formation. *Nature* **463**, 958–962 (2010).
41. A. Dubey, J.-P. Saint-Jeannet, Modeling human craniofacial disorders in *Xenopus*. *Curr. Pathobiol. Rep.* **5**, 79–92 (2017).
42. D. W. Seufert, J. Hanken, M. W. Klymkowsky, Type II collagen distribution during cranial development in Xenopus laevis. *Anat. Embryol. (Berl.)* **189**, 81–89 (1994).
43. A. Tekari, R. Luginbuehl, W. Hofstetter, R. J. Egli, Transforming growth factor beta signaling is essential for the autonomous formation of cartilage-like tissue by expanded chondrocytes. *PLoS One* **10**, e0120857 (2015).
44. C. Chadjichristos *et al.*, Down-regulation of human type II collagen gene expression by transforming growth factor-beta 1 (TGF-beta 1) in articular chondrocytes involves SP3/SP1 ratio. *J. Biol. Chem.* **277**, 43903–43917 (2002).
45. P. S. Albert, D. L. Riddle, Mutants of *Caenorhabditis elegans* that form dauer-like larvae. *Dev. Biol.* **126**, 270–293 (1988).
46. E. S. Haag, Dial-a-mutant: Web-based knockout collections for model organisms. *Biol. Cell* **99**, 343–347 (2007).
47. J. D. Hibshman, A. K. Webster, L. R. Baugh, Liquid-culture protocols for synchronous starvation, growth, dauer formation, and dietary restriction of *Caenorhabditis elegans*. *STAR Protoc* **2**, 100276 (2021).
48. P. Narbonne, R. Roy, *Caenorhabditis elegans* dauers need LKB1/AMPK to ration lipid reserves and ensure long-term survival. *Nature* **457**, 210–214 (2009).
49. P. Kadekar, R. Roy, AMPK regulates germline stem cell quiescence and integrity through an endogenous small RNA pathway. *PLoS Biol.* **17**, e3000309 (2019).
50. J. R. Berman, C. Kenyon, Germ-cell loss extends *C. elegans* life span through regulation of DAF-16 by kri-1 and lipophilic-hormone signaling. *Cell* **124**, 1055–1068 (2006).
51. H. Hsin, C. Kenyon, Signals from the reproductive system regulate the lifespan of *C. elegans*. *Nature* **399**, 362–366 (1999).
52. D. A. Garsin *et al.*, Long-lived *C. elegans* daf-2 mutants are resistant to bacterial pathogens. *Science* **300**, 1921 (2003).
53. I. Lee, A. Hendrix, J. Kim, J. Yoshimoto, Y.-J. You, Metabolic rate regulates L1 longevity in *C. elegans*. *PLoS One* **7**, e44720 (2012).
54. M. Ailion, J. H. Thomas, Dauer formation induced by high temperatures in *Caenorhabditis elegans*. *Genetics* **156**, 1047–1067 (2000).
55. A. J. Schindler, L. R. Baugh, D. R. Sherwood, Identification of late larval stage developmental checkpoints in *Caenorhabditis elegans* regulated by insulin/IGF and steroid hormone signaling pathways. *PLoS Genet.* **10**, e1004426 (2014).
56. C. Savage *et al.*, *Caenorhabditis elegans* genes sma-2, sma-3, and sma-4 define a conserved family of transforming growth factor beta pathway components. *Proc. Natl. Acad. Sci. U.S.A.* **93**, 790–794 (1996).
57. Y. Suzuki *et al.*, A BMP homolog acts as a dose-dependent regulator of body size and male tail patterning in *Caenorhabditis elegans*. *Development* **126**, 241–250 (1999).
58. K. Morita, K. L. Chow, N. Ueno, Regulation of body length and male tail ray pattern formation of *Caenorhabditis elegans* by a member of TGF-beta family. *Development* **126**, 1337–1347 (1999).
59. B. Gerisch, C. Weitzel, C. Kober-Eisermann, V. Rottiers, A. Antebi, A hormonal signaling pathway influencing *C. elegans* metabolism, reproductive development, and life span. *Dev. Cell* **1**, 841–851 (2001).
60. R. P. Boot-Handford, D. S. Tuckwell, Fibrillar collagen: The key to vertebrate evolution? A tale of molecular incest. *BioEssays* **25**, 142–151 (2003).
61. W. R. Wilcox, Connective tissue and its heritable disorders: Molecular, genetic, and medical aspects. *Am. J. Hum. Genet.* **72**, 503–504 (2003).
62. A. Wood, D. E. Ashhurst, A. Corbett, P. Thorogood, The transient expression of type II collagen at tissue interfaces during mammalian craniofacial development. *Development* **111**, 955–968 (1991).
63. C. Baugé, O. Cauvard, S. Leclercq, P. Galéra, K. Boumédiene, Modulation of transforming growth factor beta signalling pathway genes by transforming growth factor beta in human osteoarthritic chondrocytes: Involvement of Sp1 in both early and late response cells to transforming growth factor beta. *Arthritis Res. Ther.* **13**, R23 (2011).
64. R. Kerney, B. K. Hall, J. Hanken, Regulatory elements of Xenopus col2a1 drive cartilaginous gene expression in transgenic frogs. *Int. J. Dev. Biol.* **54**, 141–150 (2010).
65. J. R. Siebert, J. M. Graham Jr., C. MacDonald, Pathologic features of the CHARGE association: Support for involvement of the neural crest. *Teratology* **31**, 331–336 (1985).
66. A. Antebi, W. H. Yeh, D. Tait, E. M. Hedgecock, D. L. Riddle, daf-12 encodes a nuclear receptor that regulates the dauer diapause and developmental age in *C. elegans*. *Genes Dev.* **14**, 1512–1527 (2000).
67. S. So, K. Miyahara, Y. Ohshima, Control of body size in *C. elegans* dependent on food and insulin/IGF-1 signal. *Genes Cells* **16**, 639–651 (2011).
68. T. Del Rio-Albrechtsen, K. Kiontke, S.-Y. Chiou, D. H. A. Fitch, Novel gain-of-function alleles demonstrate a role for the heterochronic gene lin-41 in *C. elegans* male tail tip morphogenesis. *Dev. Biol.* **297**, 74–86 (2006).
69. M. Fujiwara, P. Sengupta, S. L. McIntire, Regulation of body size and behavioral state of *C. elegans* by sensory perception and the EGL-4 cGMP-dependent protein kinase. *Neuron* **36**, 1091–1102 (2002).
70. M. Murakami, M. Koga, Y. Ohshima, DAF-7/TGF-β expression required for the normal larval development in *C. elegans* is controlled by a presumed guanylyl cyclase DAF-11. *Mech. Dev.* **109**, 27–35 (2001).
71. Y. Liu *et al.*, CHD7 interacts with BMP R-SMADs to epigenetically regulate cardiogenesis in mice. *Hum. Mol. Genet.* **23**, 2145–2156 (2014).
72. M. Tewari, *et al.*, Systematic interactome mapping and genetic perturbation analysis of a *C. elegans* TGF-beta signaling network. *Mol. Cell*, **13**, 469–482.
73. C. G. Riedel *et al.*, DAF-16 employs the chromatin remodeller SWI/SNF to promote stress resistance and longevity. *Nat. Cell Biol.* **15**, 491–501 (2013).
74. K. Jia, P. S. Albert, D. L. Riddle, DAF-9, a cytochrome P450 regulating *C. elegans* larval development and adult longevity. *Development* **129**, 221–231 (2002).
75. X. Chu *et al.*, Genotranscriptomic meta-analysis of the CHD family chromatin remodelers in human cancers - initial evidence of an oncogenic role for CHD7. *Mol. Oncol.* **11**, 1348–1360 (2017).
76. R. A. C. Machado *et al.*, CHD7 promotes glioblastoma cell motility and invasiveness through transcriptional modulation of an invasion signature. *Sci. Rep.* **9**, 3952 (2019).
77. M. B. Sporn *et al.*, Polypeptide transforming growth factors isolated from bovine sources and used for wound healing in vivo. *Science* **219**, 1329–1331 (1983).
78. A. B. Roberts *et al.*, Transforming growth factor type beta: Rapid induction of fibrosis and angiogenesis in vivo and stimulation of collagen formation in vitro. *Proc. Natl. Acad. Sci. U.S.A.* **83**, 4167–4171 (1986).
79. M. Laiho, O. Saksela, P. A. Andreasen, J. Keski-Oja, Enhanced production and extracellular deposition of the endothelial-type plasminogen activator inhibitor in cultured human lung fibroblasts by transforming growth factor-beta. *J. Cell Biol.* **103**, 2403–2410 (1986).
80. C. M. Overall, J. L. Wrana, J. Sodek, Independent regulation of collagenase, 72-kDa progelatinase, and metalloendoproteinase inhibitor expression in human fibroblasts by transforming growth factor-β. *J. Biol. Chem.* **264**, 1860–1869 (1989).
81. M. Breuer, M. Rummler, C. Zaouter, B. M. Willie, S. A. Patten, Abnormal craniofacial and spinal bone development with col2a1a depletion in a zebrafish model of CHARGE syndrome. *bioRxiv* [Preprint] (2020). https://www.biorxiv.org/content/10.1101/2020.07.10.197533v3 (Accessed 29 March 2022).
82. T. Suzuki, D. Sakai, N. Osumi, H. Wada, Y. Wakamatsu, Sox genes regulate type 2 collagen expression in avian neural crest cells. *Dev. Growth Differ.* **48**, 477–486 (2006).
83. D. He *et al.*, Chd7 cooperates with Sox10 and regulates the onset of CNS myelination and remyelination. *Nat. Neurosci.* **19**, 678–689 (2016).
84. C. L. Hale, A. N. Niederriter, G. E. Green, D. M. Martin, Atypical phenotypes associated with pathogenic CHD7 variants and a proposal for broadening CHARGE syndrome clinical diagnostic criteria. *Am. J. Med. Genet. A.* **170A**, 344–354 (2016).
85. S. K. Han *et al.*, OASIS 2: online application for survival analysis 2 with features for the analysis of maximal lifespan and healthspan in aging research. *Oncotarget* **7**, 56147–56152 (2016).
86. P. D. Nieuwkoop, J. Faber, *Normal Table of Xenopus laevis (Daudin)* (Garland Publishing, 1994).
87. S. Huang, K. E. Johnson, H. Z. Wang, Blastomeres show differential fate changes in 8-cell Xenopus laevis embryos that are rotated 90 degrees before first cleavage. *Dev. Growth Differ.* **40**, 189–198 (1998).
88. V. Gawantka *et al.*, Gene expression screening in Xenopus identifies molecular pathways, predicts gene function and provides a global view of embryonic patterning. *Mech. Dev.* **77**, 95–141 (1998).
89. National Research Council, *Guide for the Care and Use of Laboratory Animals* (National Academies Press, Washington, DC, ed. 8, 2011).
90. N. Zahn, M. Levin, D. S. Adams, The Zahn drawings: New illustrations of *Xenopus* embryo and tadpole stages for studies of craniofacial development. *Development* **144**, 2708–2713 (2017).